

Interparticle Delivery and Detection of Volatile Singlet Oxygen at Air/Solid Interfaces

Andrés M. Durantini* and Alexander Greer*



Cite This: *Environ. Sci. Technol.* 2021, 55, 3559–3567



Read Online

ACCESS |



Metrics & More

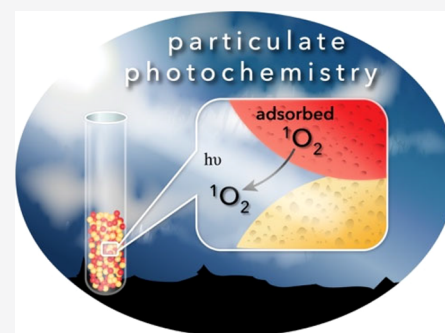


Article Recommendations



Supporting Information

ABSTRACT: An interparticle system has been devised, allowing airborne singlet oxygen to transfer between particle surfaces. Singlet oxygen is photogenerated on a sensitizer particle, where it then travels through air to a second particle bearing an oxidizable compound—a particulate-based approach with some similarities to reactive oxygen quenching in the atmosphere. In atmospheric photochemistry, singlet oxygen is generated by natural particulate matter, but its formation and quenching between particles has until now not been determined. Determining how singlet oxygen reacts on a second surface is useful and was developed by a three-phase system (particle–air–particle) *interparticle* photoreaction with tunable quenching properties. We identify singlet oxygen quenching directly by near-IR phosphorescence in the airborne state and at the air/particle interface for total quenching rate constants (k_T) of adsorbed anthracene trapping agents. The air/solid interface k_T of singlet oxygen by anthracene-coated particles was $(2.8 \pm 0.8) \times 10^7 \text{ g mol}^{-1} \text{ s}^{-1}$ for 9,10-dimethylanthracene and $(2.1 \pm 0.9) \times 10^7 \text{ g mol}^{-1} \text{ s}^{-1}$ for 9,10-anthracene dipropionate dianion, and the lifetime of airborne singlet oxygen was measured to be 550 μs . These real-time interactions and particle-induced quenching steps open up new opportunities for singlet oxygen research of atmospheric and particulate processes.



INTRODUCTION

Airborne reactive oxygen species (ROS) are prominent in environmental photoreactions, and scientists have become interested in their reactions on surfaces. Such ROS, including $^1\text{O}_2$, RO \cdot , HO \cdot , and $\text{O}_2^{\cdot-}$ are commonly produced by sunlight irradiation via sensitized oxidation reactions.^{1–11} Interactions of ROS can be significant in atmospheric and soil environments, such as on particulate matter (PM) and silicon dioxide.^{12–15} However, they cannot be easily detected on surfaces using direct techniques and they are often limited to analysis by indirect techniques.

Using indirect techniques, a steady-state concentration of $^1\text{O}_2$ ($[^1\text{O}_2]_{\text{ss}}$) of $1.6 \pm 0.5 \times 10^{-12} \text{ M}$ in fog was measured using furfuryl alcohol.^{16,17} Indirect studies to deduce $[^1\text{O}_2]_{\text{ss}}$ have also been carried out on air/ice interfaces¹⁸ and on water surfaces.^{19–21} The production of $^1\text{O}_2$ can arise from natural organic matter (NOM) in which their chromophores enable sensitization in water bodies exposed to sunlight.^{5,19–23} Natural chromophores in soil can absorb light and by sensitization can produce $^1\text{O}_2$.² Soil surface photooxidation was studied with $^1\text{O}_2$ traps agents, tetramethylethylene and 2,5-dimethylfuran¹⁰ with sunlight exposure. Interestingly, airborne $^1\text{O}_2$ can diffuse up to 2 mm on soil.⁹ In a historic experiment using a pressurized system, Kautsky conducted experiments in the 1930s mixing two sets of particles of different sizes containing a photosensitizer (PS) (trypaflavine) and gaseous $^1\text{O}_2$ quencher (leucomalachite green) for early evidence of $^1\text{O}_2$.^{24,25} Kautsky's experiment

was redesigned, Wolf et al. captured $^1\text{O}_2$ between two polymer surfaces,²⁶ Ruzzi et al. detected gaseous $^1\text{O}_2$ with a pressurized electron paramagnetic resonance (EPR) system,²⁷ and Naito et al.^{28,29} used indirect single molecule fluorescence detection technique to show transport of $^1\text{O}_2$ between two surfaces via air (i.e., a solid/air/solid three-phase system). Studies using EPR technique have also shown that $^1\text{O}_2$ is also involved in photochemical air pollution.^{2,30–32}

Such EPR and indirect trapping techniques can be limited in their utility as probes of $^1\text{O}_2$ at interfaces. Techniques that can directly track $^1\text{O}_2$ at interfaces by laser spectroscopy are needed to open the way to studying $^1\text{O}_2$ processes on particulates. Only a limited number of environmental studies have focused on direct $^1\text{O}_2$ detection. Recently, direct laser techniques were carried out to measure singlet oxygen quantum yields (Φ_Δ) by NOM sensitization by monitoring the $^1\text{O}_2$ phosphorescence directly³³ with Φ_Δ values of 0.6–3.8%.⁶ Only limited number of studies have focused on solid–air–solid systems^{34–36} or how airborne $^1\text{O}_2$ interacts with natural and artificial surfaces.^{9,11,37}

Received: November 24, 2020

Revised: January 21, 2021

Accepted: February 18, 2021

Published: March 4, 2021



There are needs in terms of particulate environmental photochemistry, as there are difficulties in deducing the transport of ROS between surfaces. Direct laser work on heterogeneous systems is more challenging than their solution-phase counterparts. Furthermore, it is not clear what surface effects are best suited for the generation and transfer of volatile ROS such as $^1\text{O}_2$. In the present study, we used an interparticle system for insight into how airborne $^1\text{O}_2$ transports from one surface to another and ways in which it is facilitated (Figure 1). Novel aspects of our work include advancing interfacial reactive oxygen chemistry with time-resolved air/solid $^1\text{O}_2$ direct laser work.

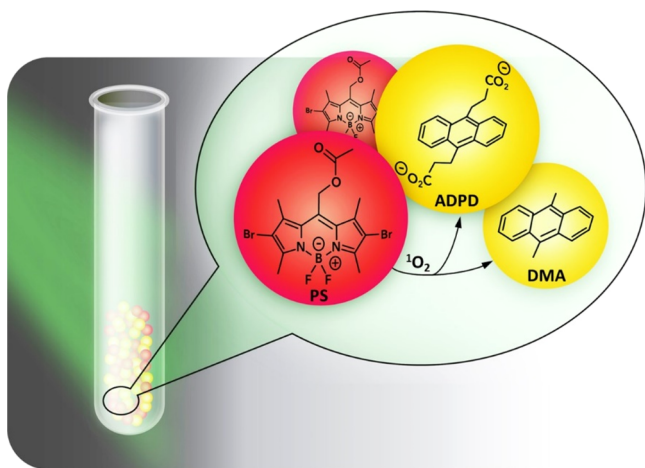


Figure 1. Interparticle transport of volatile $^1\text{O}_2$. Schematic showing the donor–acceptor interparticle $^1\text{O}_2$ migration system. Singlet oxygen diffuses through air after its generation on a photosensitizing donor particle (P_{PS} , BODIPY photosensitizer, red particles) and trapped on an acceptor particle (P_Q , anthracene quenchers DMA or ADPD, yellow particles).

We hypothesized that a sensitizer particle (P_{PS}) will generate $^1\text{O}_2$ and the $^1\text{O}_2$ is delivered through air to another particle bearing an oxidizable quencher (P_Q) in a three-phase manner (particle–air–particle). The results demonstrate an interfacial $^1\text{O}_2$ production, where air/solid interface total quenching rate constants ($ASI-k_T$) and singlet oxygen quantum yields (Φ_Δ) are measured by direct phosphorescence via an interparticle method.

We report here a study of a three-phase (particle–air–particle) system involving $^1\text{O}_2$. A mechanism, which involves the reaction of airborne $^1\text{O}_2$ with particle-adsorbed anthracene, is proposed (Figure 2). This study provides the first direct evidence for a mechanism involving interfacial and airborne $^1\text{O}_2$. Porous Vycor glass (PVG) particles were coated with an 8-acetoxymethyl-2,6-dibromo-1,3,5,7-tetramethyl pyromethene fluoroborate (BODIPY, $\text{Br}_2\text{B-OAc}$) sensitizer (P_{PS}), which are irradiated with a 532 nm light from a Nd:YAG laser. This BODIPY PS was chosen because it has increased photostability compared to its *bis*-iodinated analog $\text{I}_2\text{B-OAc}$ or conventional sensitizers such as rose bengal.³⁸ The triplet excited state of the BODIPY PS on the particle is quenched by $^3\text{O}_2$ in an energy transfer process to generate $^1\text{O}_2$. The resulting $^1\text{O}_2$ phosphorescence was monitored at 1270 nm, which exhibited remarkably different lifetimes on the particles and as a free species in air. The quenching of $^1\text{O}_2$ arises on particles adsorbed with anthracene quenchers (P_Q). The particles P_Q were coated with quenching

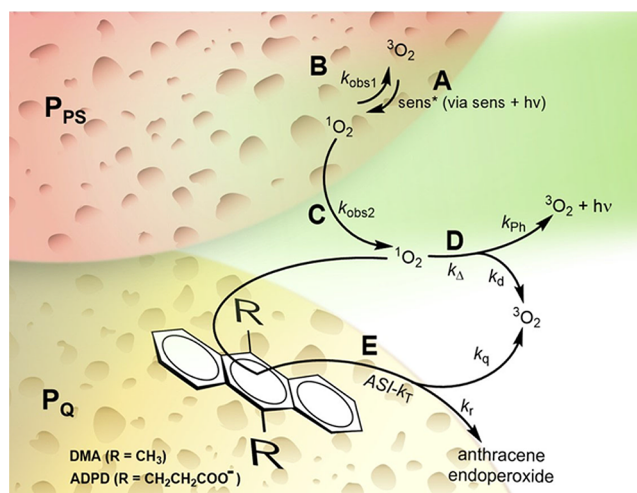


Figure 2. The interparticle reaction is a triphasic (particle–air–particle) system, which segregates a sensitizer particle from an acceptor particle for quenching of the generated airborne $^1\text{O}_2$. (A) Formation of $^1\text{O}_2$ by the excited photosensitizer particle (P_{PS}), (B) physical quenching of $^1\text{O}_2$ to $^3\text{O}_2$ ($k_{\text{obs}1}$) by the P_{PS} particle surface, (C) detection of airborne $^1\text{O}_2$ ($k_{\text{obs}2}$) in which (D) radiative and non-radiative deactivation of $^1\text{O}_2$ in air is dominated by physical quenching and phosphorescence, and (E) reaction of $^1\text{O}_2$ with the anthracene trap on a separate particle (P_Q) to form an anthracene endoperoxide with $^1\text{O}_2$. Airborne $^1\text{O}_2$ can travel tenths of millimeter distances between P_{PS} and P_Q . There is no interparticle transfer of the sensitizer and anthracene traps.

agents 9,10-anthracene dipropionate dianion (ADPD) or 9,10-dimethylanthracene (DMA), enabling $ASI-k_T$ and Φ_Δ determinations. Our interparticle system offers a mechanistic tool to analyze $^1\text{O}_2$ migration through air and its reaction at the air/solid interface of a second surface. There is novelty in the present air/particle and airborne $^1\text{O}_2$ laser work due to the lack of such direct measurements in the environmental chemistry literature. The work comprises of an interfacial air/solid and airborne $^1\text{O}_2$ detection system. The experimental data collected are consistent with the mechanism shown in Figure 2, as we describe below.

MATERIALS AND METHODS

Materials and Instrumentation. Corning 7930 porous Vycor glass (PVG), purchased from Advanced Glass and Ceramics, Holden, MA, was ground and sieved to particles (diameter 100–200 μm). PVG has a surface area of 250 m^2/g , it is a porous material with an average pore diameter of 4 nm.⁴² Acetonitrile and dichloromethane were purchased from Sigma-Aldrich and used as received. Deionized water was purified using a U.S. Filter Corp. deionization system (Vineland, NJ, USA). UV–visible spectra were collected on an Agilent spectrophotometer.

Singlet Oxygen Phosphorescence at the Air–Solid Interface and in Air. The photosensitization of $^1\text{O}_2$ by the P_{PS} particles was demonstrated by measuring its phosphorescence upon irradiation of the sample with a Nd:YAG Q-switched laser producing 532 nm with an ~ 4 ns fwhm. The laser was operating at 5 Hz and 30 mJ/pulse, and 6 laser pulses were applied to acquire a trace. The $^1\text{O}_2$ phosphorescence was detected using a photomultiplier tube (H10330A-45 Hamamatsu Corp.) operating at a voltage of -650 V using a NIR band-pass filter centered at 1270 nm (OD4 blocking, fwhm = 15 nm). The signals were registered on a 600 MHz oscilloscope, and the kinetic data for all

the samples containing the PS were fitted with a biexponential function. An open quartz cuvette with a 10 mm path length containing 100 mg of P_{PS} or 100 mg of P_{PS} + 100 mg of P_Q particles was irradiated from the top, reflecting the laser beam on a right-angle prism. Samples were purged with N_2 or air using a septum screw-capped quartz cuvette and were irradiated from the bottom by reflecting the laser beam. For the Φ_{Δ} measurements, the frequency was increased to 10 Hz and the power decreased to 10 mJ/pulse to avoid rapid photobleaching of the dye, also, the signal of 3 laser pulses were averaged to acquire a trace. Further detail on the apparatus design is provided in the Supporting Information. Here, apparatus dosing and optimization permitted to increase excitation power and the time resolution due to 6 order of magnitude increase in the surface area.

Design of Airborne 1O_2 Quenching System at Air/Solid Interfaces. Particles containing the Br_2B-OAc PS were prepared as described in the Supporting Information. The PS loading was 0.050 $\mu\text{mol/g}$ of PVG particles. Stock solutions of the quenchers were prepared in H_2O (pH = 10) for ADPD and in acetonitrile for DMA. Different volumes of the quenchers were added in 5 vials containing 200 mg of particles to achieve the desired loading. The solvents were removed under vacuum in a rotary evaporator operating at 50 mbar, and the samples were dried in an oven with reduced pressure for 1 h at 60 $^{\circ}C$. To acquire the trace corresponding to the decay of 1O_2 phosphorescence, 100 mg of P_{PS} was mixed with 100 mg of P_Q containing the desired quencher and loading.

RESULTS AND DISCUSSION

“Lightening Up” Singlet Oxygen for Transport between Particles. We sought an optimal 1O_2 photo-generation by the PS particles to allow a view of the through-space 1O_2 process. In a previous study,³⁴ we were not able to obtain direct lifetime measurements for airborne 1O_2 generated on a superhydrophobic surface embedded with phthalocyanine particles. On that occasion, due to low phosphorescence emission, time resolution was not possible and only variations in the intensity were monitored. Here, we varied PS loading with emission and absorbance of Br_2B-OAc molecules (Figure S1, Supporting Information) that overlap by $\sim 30\%$ to avoid close proximity from high loading, <50 nm, where photoexcited sensitizer self-quenches by Förster resonance energy transfer (FRET).^{39–41} Low PS loading is also undesirable due to low signal-to-noise ratios. Both under- and overloading of PS will lead to less triplet excited states, and thus less airborne 1O_2 . A loading of 0.050 μmol PS per gram of particle ($\mu\text{mol/g}$) was found to be the optimal amount of PS adsorbed on the glass surface. The distance between PS molecules under these conditions was calculated to be 180 nm. Another consideration is that the PS remains embedded within the pores. Under this circumstance, the surface area is reduced to 70 m^2/g and the PS-PS distance to 94 nm. The average distance between PS molecules was calculated by estimating the area occupied by the molecule (Figure S2) relative to the surface area of a particle. Based on these calculations, we predict that an optimal PS loading is 0.050 $\mu\text{mol/g}$ for a compromise to maximize 1O_2 formation due to sufficiently high PS amounts, and yet minimize unwanted PS/PS self-quenching by FRET.

This was tested experimentally. Figure 3A shows the 1O_2 phosphorescence decay curves for 100 mg of P_{PS} with different PS loadings and the controls (native particles and P_{non-PS} loaded with 0.050 $\mu\text{mol/g}$ of H_2B-OAc , which gives no 1O_2

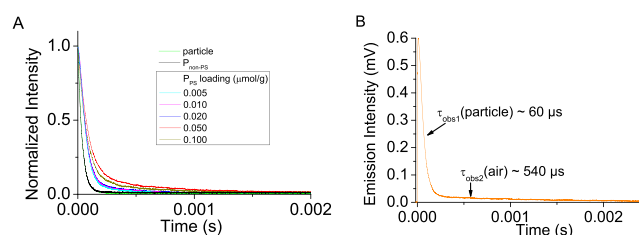


Figure 3. (A) Airborne 1O_2 decay curves photosensitized by P_{PS} particles loaded with varying amounts of photosensitizer (PS) (0.005–0.1 $\mu\text{mol/g}$ particle). The decay curves for the native (uncoated) particles and the “non-photosensitizer” coated particle P_{non-PS} (0.050 $\mu\text{mol/g}$ particle) are also shown. (B) Decay curve showing the two 1O_2 lifetimes (τ_{obs1} and τ_{obs2}) from the bi-exponential fitting of the data for the interparticle 1O_2 exchange system. Intensity decay was monitored at 1270 nm.

production). Fitting of the intensity vs time with a bi-exponential function (eq S1, Supporting Information) led to two distinct lifetimes (Figure 3B). The data in Table 1 support

Table 1. Singlet Oxygen Lifetimes Obtained from the Intensity Decays Curves for the Controls and Different Particle Loadings of the PS

entry	PS loading ($\mu\text{mol sens/g particle}$)	τ_{obs1} (μs) ^b	τ_1 (μs) ^b	τ_{obs2} (μs) ^b
1 ^a	0.005	50.3	15.2	373
2 ^a	0.010	52.1	17.0	426
3 ^a	0.020	53.5	18.4	432
4 ^a	0.050	58.5	23.4	537
5 ^a	0.100	55.2	20.2	416

^aParticles coated with the sensitizer Br_2B-OAc . ^bErrors for the short lifetimes are ± 1 μs and for the long lifetimes ± 5 –10 μs , and the error ranges for fitting are 0.01–0.03 μs . Values for τ_{bckgrd} are 35.1 and 34.8 μs for native particles and P_{non-PS} , respectively.

the identification of two lifetimes: a short lifetime (τ_{obs1}) of ~ 54 μs that remained similar at various PS loadings (entries 1–5), and a longer lifetime (τ_{obs2}) that varies with the amount of PS loading and reaches a maximum of ~ 540 μs (loading 0.050 $\mu\text{mol/g}$). A mono-exponential decay from background was observed, $\tau_{bckgrd} = \sim 35$ μs , but this was not due to 1O_2 phosphorescence (eq S2, Supporting Information). This background signal corresponds to spurious light reaching the detector even when a NIR band-pass filter centered at 1270 nm was applied. The τ_{bckgrd} values showed very small variation among the different experiments bearing an experimental error of 1.0 μs . This background signal was verified not to be from 1O_2 phosphorescence by exciting native particles with constant laser power and varying the diameter of the NIR detector iris causing some light to reach the detector (Figure S3). Were the signal due to 1O_2 , the signal intensity would have varied and the lifetime would have remained essentially constant. Figure 3A,B shows conditions that led to an enhanced signal to get the best 1O_2 signal-to-background ratio. With this data in hand, a lifetime τ_1 is attributed to adsorbed 1O_2 and is the difference between τ_{obs1} and $\tau_{control}$ for native particles (Table 1). As we will see next, the long lifetime is attributable to airborne 1O_2 .

The 1O_2 Particulate Quenching Connection. Direct detection reveals two lifetimes attributable to particle adsorbed 1O_2 and airborne 1O_2 (Table 2). Our experiments were carried out in the presence of air and by sparging with N_2 . Sparging a 100 mg of P_{PS} with N_2 for 15 min, as seen in Figure 4, led to a

Table 2. Singlet Oxygen Lifetimes from the 1270 nm Intensity Decay Curves under Various Conditions

entry	condition	τ_{obs1} (μs) ^b	τ_1 (μs) ^b	τ_{obs2} (μs) ^b
1 ^a		61.2	24.8	560
2	pre-purge with N ₂	65.9	29.5	
3	re-oxygenation	58.1	21.7	475
4	200 μL H ₂ O	40.2	3.8	
5	20 mg ADPD	55.7	19.3	

^aP_{PS} particles under ambient conditions. ^bErrors for the short lifetimes are typically $\pm 1 \mu\text{s}$ and for the long lifetimes $\pm 5\text{--}10 \mu\text{s}$. The fitting errors range from 0.01 to 0.03 μs . The value for τ_{backgrd} is 36.4 μs for native particles.

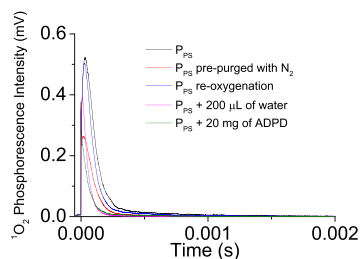


Figure 4. Airborne ¹O₂ decay monitored upon photoexcitation of P_{PS} particles in the presence of different quenchers. The loading was 0.050 μmol ADPD per gram particle, and the intensity decay was monitored at 1270 nm.

disappearance of the long lifetime component with only the short lifetime remaining ($\tau_{\text{obs1}} = 65.9 \mu\text{s}$), where this value in entry 2 is due to trace O₂ remaining adsorbed to the particle.⁴³ The slightly higher value of 65.9 μs compare to the $\sim 60 \mu\text{s}$ for P_{PS} (Table 2, entry 2) in ambient conditions can be attributed to a reduction of humidity after purging with the inert gas. After 15 min of re-oxygenation of the particles with flowing air, the two lifetimes were recovered (Table 2, entry 3). On the other hand, τ_{obs1} and τ_{obs2} reduced or disappeared (entry 4) due to adsorbed water molecules, where ¹O₂ is readily quenched. Indeed, we find that $\tau_1 = 3.8 \mu\text{s}$ (Table 2, entry 4), which matches the known lifetime of ¹O₂ in water.^{35,44} An experiment was carried out by incorporating quenchers to the particles. The phosphorescence signal was analyzed with the addition of ADPD (Figure 1), a water-soluble anthracene derivative. Singlet oxygen reacts with anthracenes to give endoperoxides.^{45–47} The addition of P_{PS} coated with ADPD (20 mg) resulted again in the loss of τ_{obs2} (Table 2, entry 5). The τ_1 was $\sim 5 \mu\text{s}$ lower with respect to P_{PS} with a value of 19.3 μs , indicating that the quencher deactivates adsorbed ¹O₂ only to a minor extent.

Interparticle Control of Airborne ¹O₂ Reactions. Next, control reactions were carried out to test the possibility of whether the donor and the acceptor migrate between particles. The results show that no molecule crossover occurred based on absorption spectroscopy measurements (Figure 5 and Figure S4), as the reaction requires. With an instrument detection limit of 0.01 (absorbance) and the molar absorptivity of 9000 M⁻¹ cm⁻¹ and 81,000 M⁻¹ cm⁻¹ for ADPD and Br₂B-OAc, respectively, we estimate a detection limit of 1.11 and 0.12 μM . With a cuvette volume of 1.5 mL, the detection limit for ADPD and Br₂B-OAc is 1.67 and 0.18 nmol, respectively. These amounts unable to account for the observed singlet oxygenation. Thus, the data support a reaction in which there is no exchange of compounds between P_{PS} and P_Q particles, whereas ¹O₂ freely migrates through space and between the particles.

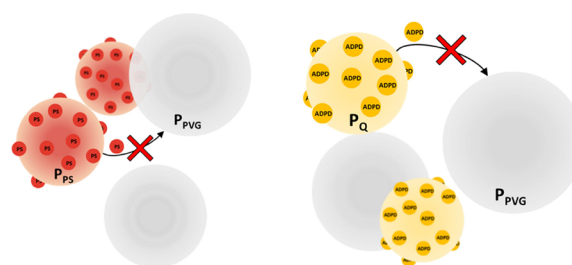


Figure 5. Particles size 38 μm > particle < 100 μm containing the PS (left) or the quencher ADPD (right) were mixed with native particles size 100 μm > particle < 800 μm to evaluate molecules exchange between particles. PS loading: 0.125 $\mu\text{mol/g}$; ADPD loading: 0.125 $\mu\text{mol/g}$.

Control reactions also demonstrated that particle size did not strongly influence the production of ¹O₂. It is known that particles of different sizes can influence light scattering and this can affect our background signal between samples.^{48–50} From our analysis, varying the P_{PS} particles size from an ~ 70 to >800 μm , showed no significant difference in the ¹O₂ phosphorescence decay curves with τ_{obs1} and τ_{obs2} values of 59 and 542 μs , respectively (see Supporting Information for experimental details, Figure S5 and Table S1).

Singlet Oxygen Quantum Yield (Φ_{Δ}). The Φ_{Δ} was measured for the P_{PS} particles by monitoring the increase in the ¹O₂ phosphorescence as a function of the irradiation time. P_{PS} particles were mixed with P_Q particles containing a loading of 50 $\mu\text{mol/g}$ DMA. As can be observed in Figure 6 and Table S2, the

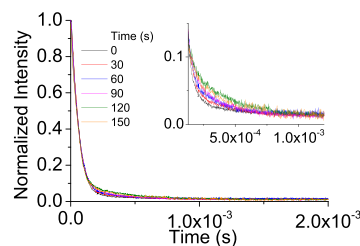


Figure 6. Normalized intensity decay curves of photoexcited mixtures of P_{PS}:P_Q (1:1) particles. The quencher loading was kept constant at 50 $\mu\text{mol/g}$ and the samples were irradiated for different times. P_{PS} = 0.050 $\mu\text{mol/g}$. Experiments were done in ambient conditions. Inset: zoom in of the normalized intensity decay curves between 1.3×10^{-4} and 1.2×10^{-3} s showing an intensity enhancement over time.

short component (τ_{obs1}) of the phosphorescence decay traces remained similar with the irradiation time. The τ_{obs2} increased by 58% (Table S2) upon 150 s of irradiation with a Nd:YAG laser operating at 532 nm, 10 Hz, and 10 mJ/pulse. The increase in the τ_{obs2} from 320 to 550 μs is attributed to the presence of the anthracene (DMA) trapping agent (50 $\mu\text{mol/g}$) to quench ¹O₂ in the former. Because anthracene trapping agents are known to mainly quench ¹O₂ chemically and not physically,^{45,47,51,52} the approximate DMA consumption as a function of the irradiation time and particle density permitted conversion of units from $\mu\text{mol/g}$ to molar. Similar to the indirect determination of the Φ_{Δ} , a pseudo-first-order kinetic for this reaction was proposed (eqs S3–S6). Plots of $\ln[\text{DMA}]_0/[\text{DMA}]$ vs irradiation time indicated that the conversion of DMA followed a pseudo-first-order kinetics with the irradiation time (Figure 7). By a linear fit of the data in Figure 7, it was possible to determine the observed rate constant (k_{obs}). Since there is no k_{obs} value for a

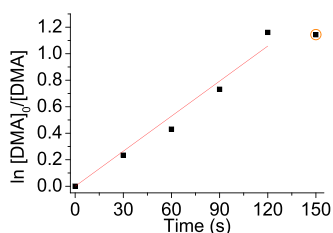


Figure 7. Pseudo-first-order kinetic data fitting for the reaction of airborne $^1\text{O}_2$ with DMA loaded onto particles [P_{DMA} ($50 \mu\text{mol/g}$) and P_{PS} ($0.050 \mu\text{mol/g}$)]. The square highlighted with an orange circle was not included in the fitting and indicates that a plateau was reached after 120 s of irradiation as a result of the consumption of the DMA quencher.

photosensitizer in a similar system to be used as a reference, we compared our k_{obs} ($8.8 \times 10^{-3} \text{ s}^{-1}$) value with that obtained for $\text{Br}_2\text{B-OAc}$ in acetonitrile $k_{\text{obs}} = 9.0 \times 10^{-3} \text{ s}^{-1}$. To determine Φ_{Δ} in this work, the k_{obs} in solid P_{PS} particles was compared with k_{obs} obtained for the same PS in solution (acetonitrile). Light scattering can be significant in solid samples compared to homogeneous solution and depends on the refractive index.^{53,54} In our case, the Φ_{Δ} with $\tau_{\text{obs}2}$ shows little or no effect from scattering unlike $\tau_{\text{obs}1}$, which shows a pronounced effect from scattering (see section PS loading optimization, above). For example, $\tau_{\text{obs}1}$ is perturbed by 50%, whereas $\tau_{\text{obs}2}$ is perturbed by less than 4%. In eq S7, the value for the refractive index of acetonitrile (1.34)⁵⁵ was used for η_{st} (st = acetonitrile standard). Meanwhile, the value for η_{PPS} was considered to be 1.00 and the air/solid Φ_{Δ} was treated as a standard-like system. The Φ_{Δ} for the P_{PS} particles was found to be 0.58 and is consistent ($\sim 25\%$ smaller) with the previously reported in solution by us and others (0.79).⁵⁶ Irradiation of the sample above 150 s resulted in a considerable amount of dye photobleaching, indicated by a significant decrease in the signal intensity (Figure S6). Furthermore, $\tau_{\text{obs}2}$ plateaus for irradiation periods longer than 120 s (orange trace in Figure 6 and Table S2) can be attributed not only to PS bleaching but also to complete consumption of the DMA on particles due to airborne $^1\text{O}_2$ produced from nearby P_{PS} particles.

Rate Constants for Airborne $^1\text{O}_2$ Quenching by Anthracene-Coated Particles. To gain information on the generation of $^1\text{O}_2$ by P_{PS} when exposed to light, we developed a quenching assay that consisted on monitoring the $^1\text{O}_2$ phosphorescence intensity decrease upon the loading of the anthracene quencher onto the particles. Quencher particles (P_{Q}) were prepared by adding two anthracene derivatives: DMA and ADPD (Figure 1). DMA is soluble in organic solvents such as ACN and toluene, while ADPD is water soluble at basic pH and used as in homogeneous solution^{47,57} but not as $^1\text{O}_2$ trapping agents at the air/particle interface as described here. For our experiments, 100 mg of P_{PS} was mixed with 100 mg of P_{Q} particles containing increasing loadings of the corresponding quencher in an open quartz cuvette.

The $^1\text{O}_2$ phosphorescence intensity vs time for different loadings of DMA and ADPD are shown in Figure 8A,B, respectively. Figure 8 and Table 3 show the decay for the short component remains constant ($\sim 60 \mu\text{s}$) in the absence of the anthracene quenchers. Fittings of the data at shorter times scales are shown in Figures S7 and S8 (Supporting Information). This is consistent with $^1\text{O}_2$ deactivation by native particles bearing Si—OH groups since $^1\text{O}_2$ can undergo quenching via electronic to vibronic (e-to-v) exchange energy transfer from O—H bond

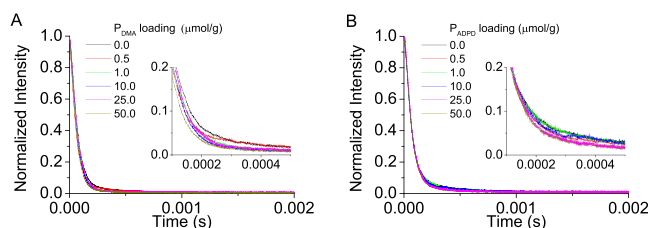


Figure 8. Normalized intensity decay curves of photoexcited mixtures of $\text{P}_{\text{PS}}:\text{P}_{\text{Q}}$ (1:1) particles increasing the quenchers loading of (A) DMA and (B) ADPD. The insets show shorter times scales. The photosensitizer loading for P_{PS} was kept at $0.050 \mu\text{mol/g}$. Experiments were done in ambient conditions. Intensity decay was monitored at 1270 nm.

Table 3. Lifetime Measurements for Singlet Oxygen Formation and Quenching in $\text{P}_{\text{PS}}:\text{P}_{\text{Q}}$ (1:1) Particle Mixtures

quencher loading ($\mu\text{mol/g}$)	DMA		ADPD	
	$\tau_{\text{obs}1}^a$ (μs)	$\tau_{\text{obs}2}^b$ (μs)	$\tau_{\text{obs}1}^a$ (μs)	$\tau_{\text{obs}2}^b$ (μs)
0 ^a	60.8	559	59.2	552
0.5	56.6	556	57.6	544
1	57.8	547	58.6	543
10	56.5	493	57.6	502
25	59.1	413	60.3	436
50	57.8	313	59.6	343

^a P_{PS} particles when mixed with native particles average size ($69 \mu\text{m}$) in a 1:1 ratio. ^bErrors for the short lifetimes are typically $\pm 1 \mu\text{s}$ and for the long lifetimes $\pm 5\text{--}10 \mu\text{s}$, and fitting error ranges from 0.01 to 0.03 μs .

oscillators.⁵⁸ However, this e-to-v quenching path is not noticeably significant since the addition of native particles do not affect the lifetime of airborne $^1\text{O}_2$, for example, $\tau_{\text{obs}2}$ for P_{PS} ($560 \mu\text{s}$, Table 2) with the value obtained in Table 3 for a mixture $\text{P}_{\text{PS}}:\text{P}_{\text{native}}$ (1:1) ($559 \mu\text{s}$). There is a significant decrease in $\tau_{\text{obs}2}$ in the presence of the particles bearing adsorbed anthracene compounds. The lifetime for the long component decreased 1.8 and 1.6 times upon the addition of the P_{Q} particles of DMA and ADPD, respectively ($50 \mu\text{mol}$ per gram particle).

The rate constants for deactivation of airborne $^1\text{O}_2$ is predicted by eq 1,

$$k_{\text{obs}2} = k_{\text{d}} + (\text{ASI} - k_{\text{T}}) [\text{Q}] \quad (1)$$

and as demonstrated by the plot shown in Figure 9, where $\text{ASI} - k_{\text{T}}$ is the air/solid interface total rate constant of $^1\text{O}_2$ by the anthracene trapping agents adsorbed on the particles, $[\text{Q}]$ is the concentration of DMA or ADPD (expressed as μmol of quencher per gram particle), and k_{d} is the rate constant of deactivation of $^1\text{O}_2$ on the particle or in air. $\text{ASI} - k_{\text{T}}$ values for an interparticle or other air/particle configuration have not been reported in the past. These results will provide insights on the efficiency of $^1\text{O}_2$ delivery through space and its quenching by compounds at a surface. From the relationship with $1/\tau_{\text{obs}2}$, $k_{\text{obs}2}$ was obtained and plotted as a function of the anthracene quencher loading (Figure 9A,B). Fitting of the data to a straight line gives the slope $\text{ASI} - k_{\text{T,DMA}} = (2.8 \pm 0.8) \times 10^7 \text{ g mol}^{-1} \text{ s}^{-1}$ ($R^2 = 0.99$) for DMA (Figure 9A) and $\text{ASI} - k_{\text{T,ADPD}} = (2.1 \pm 0.9) \times 10^7 \text{ g mol}^{-1} \text{ s}^{-1}$ ($R^2 = 0.99$) for ADPD (Figure 9B). From the intercept, k_{d} values ($\sim 1.80 \times 10^3 \text{ s}^{-1}$) were obtained, indicating a lifetime for airborne $^1\text{O}_2$ of $550 \mu\text{s}$. A somewhat similar value for

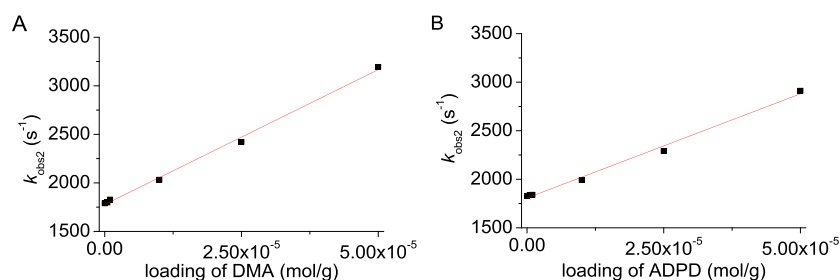


Figure 9. ASI- k_T values measured in the interparticle system. Plots of $k_{\text{obs}2}$ (s^{-1}) as a function of the moles of quencher adsorbed per gram particle (A) DMA and (B) ADPD. Experiments were performed in ambient conditions.

Table 4. Rate Constants for Total Quenching (k_T) of Anthracenes and Sulfides in Solution, at the Air/Particle Interface, or in Solution/Particle Mixtures

medium	quencher	solvent	homogeneous k_T ($\text{M}^{-1} \text{s}^{-1}$) $\times 10^7$	
homogeneous solution	DMA	MeCN	$(9.44 \pm 0.33)^a$	
	ADPD	D ₂ O	$(6.46 \pm 0.18)^a$	
	Me ₃ Si(CH ₂) ₁₀ SCH ₃	C ₆ H ₆	3.32 ^c	
medium	quencher	solid support	heterogeneous k_T	heterogeneous k_T ($\text{M}^{-1} \text{s}^{-1}$) $\times 10^4$
air/particle interface	DMA	particles	$(2.8 \pm 0.8) \times 10^7 \text{ g mol}^{-1} \text{ s}^{-1}$	2.02 ^b
	ADPD	particles	$(2.1 \pm 0.9) \times 10^7 \text{ g mol}^{-1} \text{ s}^{-1}$	1.56 ^b
solution/particle mixture	ClSiMe ₂ (CH ₂) ₁₀ SMe	silica	$27.7\text{--}29.8 \text{ L g}^{-1} \text{ s}^{-1}$	4.8–5.2 ^c

^aThis work. ^bThis work with porous Vycor glass particle and conversion using $\delta_{\text{PVG}} = 1.38 \text{ g/mL}$. ^cRef 59 with a loading of 573 μmol of ClSiMe₂(CH₂)₁₀SMe per gram silica.

gaseous ¹O₂ (980 μs) in the core of a water bubble was previously measured.^{35,36}

Mechanism. The above direct laser detection data provide a strong argument for the mechanism suggested in Figure 2. The data also provide strong evidence for interfacial and airborne ¹O₂ and reactivity of ¹O₂ at a second particle surface. The ¹O₂ phosphorescence data show its quenching on the P_{PS} particle surface itself with a short lifetime ($\sim 60 \mu\text{s}$). Singlet oxygen can transit off the particle and possesses a longer lifetime of $\sim 550 \mu\text{s}$ as an airborne species. In the absence of particle-coated anthracene, a longer-lived ¹O₂ is retained. The Φ_{Δ} for P_{PS} at the air–solid interface was determined to be 0.58 by monitoring the increase in $\tau_{\text{obs}2}$ upon consumption of an adjacent particle adsorbed with DMA. This value was slightly lower than previously reported for the Br₂B-OAc sensitizer and DMA in solution,⁵⁶ suggesting that the photophysical properties of the PS to produce ¹O₂ while adsorbed on particles largely remain intact.

The rate constant, k_T , corresponds to the anthracene compound induced to total removal of ¹O₂, which is for the first time measured at the air/particle interface. The quenching effects of ¹O₂ along the particle-adsorbed and airborne pathways are deduced. Clennan and Chen⁵⁹ have reported heterogeneous two-phase (liquid–solid) k_T values for quenching of ¹O₂ by modified surfaces of porous silica particles covalently bound to sulfides, where k_T values were between $27.7\text{--}29.8 \text{ L g}^{-1} \text{ s}^{-1}$ and “solution-phase-like” units of $\text{M}^{-1} \text{ s}^{-1}$ (Table 4). To compare with our results, our ASI- k_T values in $\text{M}^{-1} \text{ s}^{-1}$ are based on the density of PVG ($\delta = 1.38 \text{ g/mL}$).⁴² The heterogeneous k_T values are obtained in the order of $(1.5\text{--}5.2) \times 10^4 \text{ M}^{-1} \text{ s}^{-1}$, suggesting a reduced ¹O₂ accessibility to the anthracene compound at the interface compared to the solution. Furthermore, we validated the measurement of ¹O₂ quenching by DMA in acetonitrile ($9.44 \times 10^7 \text{ M}^{-1} \text{ s}^{-1}$) and by ADPD in D₂O ($6.46 \times 10^7 \text{ M}^{-1} \text{ s}^{-1}$ at pH = 10) (Figure S9). The k_T values in homogeneous solution gave very similar values to those previously reported.^{47,57}

Intriguingly, the values measured in solution are of similar magnitude to that reported for Me₃Si(CH₂)₁₀SCH₃ in benzene ($k_T = \sim 3.32 \times 10^7 \text{ M}^{-1} \text{ s}^{-1}$) (Table 4). The k_T value for sulfides in organic solvents is mostly comprised of physical quenching, but in alcohol solvents or water is mostly chemical quenching.⁶⁰ The virtues of using anthracenes are that they are efficient in chemical quenching leading to endoperoxides and that the air/particle measurements lay a “solid” foundation (pun intended) for a reference point from which to build on.

Technical Implications. The direct-detection particle–air–particle method described here produces ¹O₂, which transits off the particle and migrates through air for an oxidation reaction on a second particle surface. The photosensitizer on one particle is physically separated from the anthracene trapping agent on a second particle. Measurements of the total quenching rate constants of ¹O₂ by surface-adsorbed anthracene traps were developed. The work improves the state of the art by uncovering the mechanistic framework in Figure 2 that increase in anthracene particle loading and decreases the airborne ¹O₂ lifetime, for data that are otherwise challenging to acquire. Attributing the phosphorescence data to ¹O₂, the air/solid interface and airborne state makes this method advantageous to others, which typically use indirect or EPR trapping in homogeneous solutions or heterogeneous slurries in solution.^{61–64} The efficient transfer of ¹O₂ between particulates as a gaseous species makes this method a relevant model for a natural or artificial air/solid interface and fate of airborne ¹O₂ damage.

Our three-phase interparticle reactive oxygen delivery system provides proof of concept for particle sensitization, reactive oxygen transfer in air, and oxidative damage to adjacent solid. This particle–air–particle 3-phase system connects to fields of atmospheric chemistry, environmental chemistry, and photochemistry with surface trapping agents, and also relevance of bi- and triphasic phenomena in ¹O₂ oxidation chemistry.^{34–36,65–68} That the amount of anthracene quencher loaded was linearly dependent, provides a key reference point for compound

quenching on environmental surfaces for potential extrapolation, where trapping can increase steeply with loadings of oxophilic traps. We provide mechanistic evidence for the transfer of airborne $^1\text{O}_2$ during the photooxidation of anthracene compounds adhered to particles. We reveal through the sensitizer particle loading that airborne $^1\text{O}_2$ release and transport can be controlled. The acceptor particle is varied with loadings of anthracene trapping agents to offer a way to unveil $^1\text{O}_2$ quenching on solid surfaces. Now, we advance the state of the art with a direct phosphorescence detection technique with a particle–air–particle system, which can set the stage for opening up an area of direct methods on air–solid ROS of importance to environmental chemistry.

The results suggest important questions worthwhile of future research. It remains to be tested on how the above “artificial” particles can be compared to natural particles. It is unclear whether low phosphorescence can be observed in airborne $^1\text{O}_2$ oxidation of natural particles. Further environmental photochemistry experiments are needed, including sulfide pesticides adsorbed to soil surfaces for determination of $^1\text{O}_2$ rate constants. Future work will be required to assess the physical quenching and chemical quenching components at the air/solid interface with compounds. The technique could potentially also be utilized for airborne $^1\text{O}_2$ inactivation of soil-bound microbes at the air/solid surfaces.

We identify $^1\text{O}_2$ quenching directly by near-IR phosphorescence in the airborne state and at the air/solid interfaces with k_T measurements of adsorbed trapping agents. These direct detection and particle-induced quenching steps are amenable for further investigation, in atmospheric and particulate processes for singlet oxygen deactivation.

■ ASSOCIATED CONTENT

Supporting Information

The Supporting Information is available free of charge at <https://pubs.acs.org/doi/10.1021/acs.est.0c07922>.

PS loading in PVG particles; computational details; PS-PS distance calculation; $^1\text{O}_2$ luminescence validation at 1270 nm; effect of particle size on the production and phosphorescence of $^1\text{O}_2$, interfacial air/solid Φ_Δ ; evidence for lack of exchange of PS and ADPD molecules between particles; quenching rate constant of $^1\text{O}_2$ by DMA and ADPD in homogeneous solution, synthesis of $\text{Br}_2\text{B-OAc}$, $\text{H}_2\text{B-OAc}$, and ADPD; equations; lifetimes obtained for P_{PS} particles of different sizes and lifetimes for the mixture $\text{P}_{\text{PS}}:\text{P}_{\text{Q}}$; and normalized absorption and emission spectra of $\text{Br}_2\text{B-OAc}$, B3LYP/6-31G(d) optimized geometry of $\text{Br}_2\text{B-OAc}$, DMA and ADPD, effect of the iris diameter on the intensity decay curves, intensity decay curve of photoexcited PPS particles of different sizes absorption spectra of the solution obtained from the washings, normalized intensity decay curves of photoexcited mixtures of PPS:PQ, first-order kinetic fitting for the decays shown in Figure 8 for DMA, first-order kinetic fitting for the decays shown in Figure 8 for ADPD, and plots of k_{obs} as a function of the quencher concentration (PDF)

■ AUTHOR INFORMATION

Corresponding Authors

Andrés M. Durantini – Department of Chemistry, Brooklyn College, Brooklyn, New York 11210, United States; Ph.D.

Program in Chemistry, The Graduate Center of the City University of New York, New York 10016, United States; orcid.org/0000-0002-7898-4033; Email: adurantini@exa.unrc.edu.ar

Alexander Greer – Department of Chemistry, Brooklyn College, Brooklyn, New York 11210, United States; Ph.D. Program in Chemistry, The Graduate Center of the City University of New York, New York 10016, United States; Email: agreer@brooklyn.cuny.edu

Complete contact information is available at: <https://pubs.acs.org/10.1021/acs.est.0c07922>

Author Contributions

The manuscript was written through contributions of both authors. Both authors have given approval to the final version of the manuscript.

Notes

The authors declare no competing financial interest.

■ ACKNOWLEDGMENTS

A.M.D. and A.G. acknowledge support from the National Science Foundation (CHE-1856765). A.M.D. also acknowledges support from a Fulbright-CONICET fellowship. We thank Leda Lee for help with the graphic arts.

■ ABBREVIATIONS

PS	photosensitizer
P_{PS}	sensitizer particle
P_{Q}	quencher particle
$\text{ASI-}k_T$	total $^1\text{O}_2$ quenching rate constant
Φ_Δ	singlet oxygen quantum yield
PVG	porous Vycor glass
ADPD	9,10-anthracene dipropionate dianion
DMA	9,10-dimethylantracene
$^1\text{O}_2$	singlet oxygen
$\tau_{\text{obs}1}$	short observed lifetimes
$\tau_{\text{obs}2}$	long observed lifetime
$k_{\text{obs}1}$	observed rate constant for singlet oxygen on the surface
$k_{\text{obs}2}$	observed rate constant for airborne $^1\text{O}_2$
k_{obs}	observed rate constant of $^1\text{O}_2$ quenching by DMA
k_d	is the rate constant of deactivation of $^1\text{O}_2$ by the surrounding environment
Q	quencher

■ REFERENCES

- (1) Vione, D.; Maurino, V.; Minero, C.; Pelizzetti, E.; Harrison, M. A. J.; Olariu, R.-I.; Arsene, C. Photochemical Reactions in the Tropospheric Aqueous Phase and on Particulate Matter. *Chem. Soc. Rev.* **2006**, *35*, 441–453.
- (2) Larson, R. A.; Marley, K. A., Singlet Oxygen in the Environment. In *Environmental Photochemistry*, Boule, P., Ed. Springer: Berlin, 1999; pp. 123–137, DOI: [10.1007/978-3-540-69044-3_5](https://doi.org/10.1007/978-3-540-69044-3_5).
- (3) Zeng, T.; Arnold, W. A. Pesticide Photolysis in Prairie Potholes: Probing Photosensitized Processes. *Environ. Sci. Technol.* **2013**, *47*, 6735–6745.
- (4) Gehling, W.; Khachatryan, L.; Dellinger, B. Hydroxyl Radical Generation from Environmentally Persistent Free Radicals (EPFRs) in PM_{2.5}. *Environ. Sci. Technol.* **2014**, *48*, 4266–4272.
- (5) Braun, A. M.; Frimmel, F. H.; Hoigné, J. Singlet Oxygen Analysis in Irradiated Surface Waters. *Int. J. Environ. Anal. Chem.* **1986**, *27*, 137–149.
- (6) Partanen, S. B.; Erickson, P. R.; Latch, D. E.; Moor, K. J.; McNeill, K. Dissolved Organic Matter Singlet Oxygen Quantum Yields:

Evaluation Using Time-Resolved Singlet Oxygen Phosphorescence. *Environ. Sci. Technol.* **2020**, *54*, 3316–3324.

(7) Manfrin, A.; Nizkorodov, S. A.; Malecha, K. T.; Getzinger, G. J.; McNeill, K.; Borduas-Dedekind, N. Reactive Oxygen Species Production from Secondary Organic Aerosols: The Importance of Singlet Oxygen. *Environ. Sci. Technol.* **2019**, *53*, 8553–8562.

(8) Erickson, P. R.; Moor, K. J.; Werner, J. J.; Latch, D. E.; Arnold, W. A.; McNeill, K. Singlet Oxygen Phosphorescence as a Probe for Triplet-State Dissolved Organic Matter Reactivity. *Environ. Sci. Technol.* **2018**, *52*, 9170–9178.

(9) Hebert, V. R.; Miller, G. C. Depth Dependence of Direct and Indirect Photolysis on Soil Surfaces. *J. Agric. Food Chem.* **1990**, *38*, 913–918.

(10) Gohre, K.; Scholl, R.; Miller, G. C. Singlet Oxygen Reactions on Irradiated Soil Surfaces. *Environ. Sci. Technol.* **1986**, *20*, 934–938.

(11) Gohre, K.; Miller, G. C. Singlet Oxygen Generation on Soil Surfaces. *J. Agric. Food Chem.* **1983**, *31*, 1104–1108.

(12) Monger, C.; Kelly, E., Silica Minerals. In *Soil Mineralogy with Environmental Applications*; Soil Science Society of America: Madison, WI, USA, 2002, pp. 611–636.

(13) Eysel, W. Thermal Analysis in Earth Sciences. *Thermochim. Acta* **1987**, *110*, 495–499.

(14) McKeague, J. A.; Cline, M. G. Silica in Soil Solutions: I. The Form and Concentration of Dissolved Silica in Aqueous Extracts of Some Soils. *Can. J. Soil Sci.* **1963**, *43*, 70–82.

(15) Hans Wedepohl, K. The Composition of the Continental Crust. *Geochim. Cosmochim. Acta* **1995**, *59*, 1217–1232.

(16) Kaur, R.; Labins, J. R.; Helbock, S. S.; Jiang, W.; Bein, K. J.; Zhang, Q.; Anastasio, C. Photooxidants from Brown Carbon and Other Chromophores in Illuminated Particle Extracts. *Atmos. Chem. Phys.* **2019**, *19*, 6579–6594.

(17) Kaur, R.; Anastasio, C. Light Absorption and the Photoformation of Hydroxyl Radical and Singlet Oxygen in Fog Waters. *Atmos. Environ.* **2017**, *164*, 387–397.

(18) Hullar, T.; Magadia, D.; Anastasio, C. Photodegradation Rate Constants for Anthracene and Pyrene Are Similar in/on Ice and in Aqueous Solution. *Environ. Sci. Technol.* **2018**, *52*, 12225–12234.

(19) Haag, W. R.; Hoigné, J. Singlet Oxygen in Surface Waters. 3. Photochemical Formation and Steady-State Concentrations in Various Types of Waters. *Environ. Sci. Technol.* **1986**, *20*, 341–348.

(20) Scully, F. E., Jr.; Hoigné, J. Rate Constants for Reactions of Singlet Oxygen with Phenols and Other Compounds in Water. *Chemosphere* **1987**, *16*, 681–694.

(21) Tratnyek, P. G.; Hoigné, J. Oxidation of Substituted Phenols in the Environment: A QSAR Analysis of Rate Constants for Reaction with Singlet Oxygen. *Environ. Sci. Technol.* **1991**, *25*, 1596–1604.

(22) Vione, D.; Minella, M.; Maurino, V.; Minero, C. Indirect Photochemistry in Sunlit Surface Waters: Photoinduced Production of Reactive Transient Species. *Chem. – Eur. J.* **2014**, *20*, 10590–10606.

(23) Fu, H.; Ciuraru, R.; Dupart, Y.; Passananti, M.; Tinel, L.; Rossignol, S.; Perrier, S.; Donaldson, D. J.; Chen, J.; George, C. Photosensitized Production of Atmospherically Reactive Organic Compounds at the Air/Aqueous Interface. *J. Am. Chem. Soc.* **2015**, *137*, 8348–8351.

(24) Kautsky, H.; De Bruijn, H. The Explanation of the Inhibition of Photoluminescence of Fluorescent Systems by Oxygen: The Formation of Active, Diffusing Oxygen Molecules by Sensitization. *Naturwissenschaften* **1931**, *19*, 1043–1043.

(25) Kautsky, H.; Hirsch, A.; Fesch, R. Energy Transformations on Boundary Surfaces. VIII. The Significance of the Metastable State in Photosensitized Oxidations. *Ber.* **1935**, *68*, 152–162.

(26) Wolf, S.; Foote, C. S.; Rebek, J. Chemistry of Singlet Oxygen. 29. A Specific Three-Phase "Kautsky Test" for Singlet Oxygen. *J. Am. Chem. Soc.* **1978**, *100*, 7770–7771.

(27) Ruzzi, M.; Sartori, E.; Moscatelli, A.; Khudyakov, I. V.; Turro, N. J. Time-Resolved EPR Study of Singlet Oxygen in the Gas Phase. *J. Phys. Chem. A* **2013**, *117*, 5232–5240.

(28) Naito, K.; Tachikawa, T.; Cui, S.-C.; Sugimoto, A.; Fujitsuka, M.; Majima, T. Single-Molecule Detection of Airborne Singlet Oxygen. *J. Am. Chem. Soc.* **2006**, *128*, 16430–16431.

(29) Naito, K.; Tachikawa, T.; Fujitsuka, M.; Majima, T. Real-Time Single-Molecule Imaging of the Spatial and Temporal Distribution of Reactive Oxygen Species with Fluorescent Probes: Applications to TiO₂ Photocatalysts. *J. Phys. Chem. C* **2008**, *112*, 1048–1059.

(30) Pitts, J. N., Jr.; Khan, A. U.; Smith, E. B.; Wayne, R. P. Singlet Oxygen in the Environmental Sciences. Singlet Molecular Oxygen and Photochemical Air Pollution. *Environ. Sci. Technol.* **1969**, *3*, 241–247.

(31) Ogawa, S.; Fukui, S.; Hanasaki, Y.; Asano, K.; Uegaki, H.; Sumiko, F.; Ryosuke, S. Determination Method of Singlet Oxygen in the Atmosphere by Use of α -Terpinene. *Chemosphere* **1991**, *22*, 1211–1225.

(32) Suzen, S.; Gurer-Orhan, H.; Saso, L. Detection of Reactive Oxygen and Nitrogen Species by Electron Paramagnetic Resonance (EPR) Technique. *Molecules* **2017**, *22*, 181.

(33) Moor, K. J.; Schmitt, M.; Erickson, P. R.; McNeill, K. Sorbic Acid as a Triplet Probe: Triplet Energy and Reactivity with Triplet-State Dissolved Organic Matter via ¹O₂ Phosphorescence. *Environ. Sci. Technol.* **2019**, *53*, 8078–8086.

(34) Aebisher, D.; Bartusik-Aebisher, D.; Belh, S. J.; Ghosh, G.; Durantini, A. M.; Liu, Y.; Xu, Q.; Lyons, A. M.; Greer, A. Superhydrophobic Surfaces as a Source of Airborne Singlet Oxygen through Free Space for Photodynamic Therapy. *ACS Appl. Bio Mater.* **2020**, *3*, 2370–2377.

(35) Bartusik, D.; Aebisher, D.; Ghafari, B.; Lyons, A. M.; Greer, A. Generating Singlet Oxygen Bubbles: A New Mechanism for Gas–Liquid Oxidations in Water. *Langmuir* **2012**, *28*, 3053–3060.

(36) Bartusik, D.; Aebisher, D.; Lyons, A. M.; Greer, A. Bacterial Inactivation by a Singlet Oxygen Bubbler: Identifying Factors Controlling the Toxicity of ¹O₂ Bubbles. *Environ. Sci. Technol.* **2012**, *46*, 12098–12104.

(37) Clements, P.; Wells, C. H. Soil Sensitized Generation of Singlet Oxygen in the Photodegradation of Bioresmethrin. *Pestic. Sci.* **1992**, *34*, 163–166.

(38) Lincoln, R.; Durantini, A. M.; Greene, L. E.; Martínez, S. R.; Knox, R.; Becerra, M. C.; Cosa, G. Meso-Acetoxyethyl Bodipy Dyes for Photodynamic Therapy: Improved Photostability of Singlet Oxygen Photosensitizers. *Photochem. Photobiol. Sci.* **2017**, *16*, 178–184.

(39) Jacob, L. J.; Deigner, H.-P., Nanoparticles and Nanosized Structures in Diagnostics and Therapy. In *Precision Medicine*, Deigner, H.-P.; Kohl, M., Eds. Academic Press: 2018, pp. 229–252.

(40) Medintz, I. L.; Hildebrandt, N., *FRET-Förster Resonance Energy Transfer: From Theory to Applications*; John Wiley & Sons; 2013, pp. 105–163.

(41) Jones, G. A.; Bradshaw, D. S. Resonance Energy Transfer: From Fundamental Theory to Recent Applications. *Front. Phys.* **2019**, *7*, 1–19.

(42) Giaimuccio, J.; Zamadar, M.; Aebisher, D.; Meyer, G. J.; Greer, A. Singlet Oxygen Chemistry in Water. 2. Photoexcited Sensitizer Quenching by O₂ at the Water–Porous Glass Interface. *J. Phys. Chem. B* **2008**, *112*, 15646–15650.

(43) Clarkson, R. B.; Turkevich, J. The Adsorption of Oxygen on Porous Vycor Glass by an EPR Technique. *J. Colloid Interface Sci.* **1972**, *38*, 165–171.

(44) Wilkinson, F.; Helman, W. P.; Ross, A. B. Rate Constants for the Decay and Reactions of the Lowest Electronically Excited Singlet State of Molecular Oxygen in Solution. An Expanded and Revised Compilation. *J. Phys. Chem. Ref. Data* **1995**, *24*, 663–677.

(45) Lindig, B. A.; Rodgers, M. A. J. Rate Parameters for the Quenching of Singlet Oxygen by Water-Soluble and Lipid-Soluble Substrates in Aqueous and Micellar Systems. *Photochem. Photobiol.* **1981**, *33*, 627–634.

(46) Aebisher, D.; Zamadar, M.; Mahendran, A.; Ghosh, G.; McEntee, C.; Greer, A. Fiber-Optic Singlet Oxygen [¹O₂ (¹Δ_g)] Generator Device Serving as a Point Selective Sterilizer. *Photochem. Photobiol.* **2010**, *86*, 890–894.

- (47) Lindig, B. A.; Rodgers, M. A. J.; Schaap, A. P. Determination of the Lifetime of Singlet Oxygen in Water- d_2 Using 9,10-Anthracenedi-propionic Acid, a Water-Soluble Probe. *J. Am. Chem. Soc.* **1980**, *102*, 5590–5593.
- (48) Evstrapov, A. A.; Esikova, N. A.; Antropova, T. V. Study of Porous Glasses by the Methods of Optical Spectroscopy. *J. Opt. Technol.* **2008**, *75*, 266–270.
- (49) Ogawa, S. $1/\lambda^4$ Scattering of Light During the Drying Process in Porous Vycor Glass with Nano-Sized Pores. *J. Opt. Soc. Am. A* **2013**, *30*, 154–159.
- (50) Aragon, S. R.; Pecora, R. Theory of Dynamic Light Scattering from Polydisperse Systems. *J. Chem. Phys.* **1976**, *64*, 2395–2404.
- (51) Griesbeck, A. G.; Uhlig, J.; Sottmann, T.; Belkoura, L.; Strey, R. Singlet Oxygen Photooxygenation in Water/Pluronic F127 Hydrogels: Increased Reaction Efficiency Coupled with a Switch in Regioselectivity. *Chem. – Eur. J.* **2012**, *18*, 16161–16165.
- (52) Fudickar, W.; Linker, T. Theoretical Insights into the Effect of Solvents on the [4 + 2] Cycloaddition of Singlet Oxygen to Substituted Anthracenes: A Change from a Stepwise Process to a Concerted Process. *J. Phys. Org. Chem.* **2019**, *32*, No. e3951.
- (53) Han, X.; Shen, J.; Yin, P.; Hu, S.; Bi, D. Influences of Refractive Index on Forward Light Scattering. *Opt. Commun.* **2014**, *316*, 198–205.
- (54) Cardona, M.; Merlin, R., *Light Scattering in Solids IX*; Springer, 2006, pp. 1–14.
- (55) An, N.; Zhuang, B.; Li, M.; Lu, Y.; Wang, Z.-G. Combined Theoretical and Experimental Study of Refractive Indices of Water–Acetonitrile–Salt Systems. *J. Phys. Chem. B* **2015**, *119*, 10701–10709.
- (56) Durantini, A. M.; Greene, L. E.; Lincoln, R.; Martínez, S. R.; Cosa, G. Reactive Oxygen Species Mediated Activation of a Dormant Singlet Oxygen Photosensitizer: From Autocatalytic Singlet Oxygen Amplification to Chemically Controlled Photodynamic Therapy. *J. Am. Chem. Soc.* **2016**, *138*, 1215–1225.
- (57) Günther, S. G.; Lemp, M. E.; Zanocco, A. L. On the Use of 9,10-Dimethylanthracene as Chemical Rate Constant Actinometer in Singlet Molecular Oxygen Reactions. *J. Chil. Chem. Soc.* **2000**, *45*, 637–644.
- (58) Schweitzer, C.; Schmidt, R. Physical Mechanisms of Generation and Deactivation of Singlet Oxygen. *Chem. Rev.* **2003**, *103*, 1685–1758.
- (59) Clennan, E. L.; Chen, M. F. Photooxidation Kinetics in Heterogeneous Media. *J. Org. Chem.* **1995**, *60*, 6004–6005.
- (60) Clennan, E. L.; Greer, A. The Effect of Alcohols on the Photooxidative Behavior of Diethylsulfide. *J. Org. Chem.* **1996**, *61*, 4793–4797.
- (61) Forbes, M. D.; Ruberu, S. R.; Dukes, K. E. Dynamics of Spin-Polarized Radical Pairs at the Solid/Solution Interface. *J. Am. Chem. Soc.* **1994**, *116*, 7299–7307.
- (62) Forbes, M. D.; Dukes, K. E.; Myers, T. L.; Maynard, H. D.; Breivogel, C. S.; Jaspán, H. B. Time-Resolved Electron Paramagnetic Resonance Spectroscopy of Organic Free Radicals Anchored to Silica Surfaces. *J. Phys. Chem.* **1991**, *95*, 10547–10549.
- (63) Tarasov, V. F.; Jarocha, L. E.; Avdievich, N. I.; Forbes, M. D. TREPR Spectra of Micelle-Confined Spin Correlated Radical Pairs: I. Molecular Motion and Simulations. *Photochem. Photobiol. Sci.* **2014**, *13*, 439–453.
- (64) DeHaven, B. A.; Tokarski, J. T.; Korous, A. A.; Mentink-Vigier, F.; Makris, T. M.; Brugh, A. M.; Forbes, M. D.; van Tol, J.; Bowers, C. R.; Shimizu, L. S. Endogenous Radicals of Self-assembled Benzophenone Bis-urea Macrocycles: Characterization and Application as a Polarizing Agent for Solid-state DNP MAS NMR spectroscopy. *Chem. – Eur. J.* **2017**, *23*, 8315–8319.
- (65) Wang, K.-K.; Song, S.; Jung, S.-J.; Hwang, J. W.; Kim, M.-G.; Kim, J.-H.; Sung, J.; Lee, J.-K.; Kim, Y.-R. Lifetime and Diffusion Distance of Singlet Oxygen in Air under Everyday Atmospheric Conditions. *Phys. Chem. Chem. Phys.* **2020**, *22*, 21664–21671.
- (66) Sunday, M. O.; Takeda, K.; Sakugawa, H. Singlet Oxygen Photogeneration in Coastal Seawater: Prospect of Large-Scale Modeling in Seawater Surface and Its Environmental Significance. *Environ. Sci. Technol.* **2020**, *54*, 6125–6133.
- (67) Sunday, M. O.; Sakugawa, H. A Simple, Inexpensive Method for Gas-Phase Singlet Oxygen Generation from Sensitizer-Impregnated Filters: Potential Application to Bacteria/Virus Inactivation and Pollutant Degradation. *Sci. Total Environ.* **2020**, *746*, 141186.
- (68) Klaper, M.; Linker, T. Intramolecular Transfer of Singlet Oxygen. *J. Am. Chem. Soc.* **2015**, *137*, 13744–13747.